Journal of Solid State Chemistry 183 (2010) 437–443

Contents lists available at ScienceDirect

Journal of Solid State Chemistry

journal homepage: www.elsevier.com/locate/jssc

Structural, electronic and optical properties of orthorhombic $CdGeO_3$ from first principles calculations

C.A. Barboza [a], J.M. Henriques [a], E.L. Albuquerque [a], E.W.S. Caetano [b,*], V.N. Freire [c], J.A.P. da Costa [c]

[a] Departamento de Física Teórica e Experimental, Universidade Federal do Rio Grande do Norte, 59072-900 Natal, Rio Grande do Norte, Brazil
[b] Instituto Federal de Educação, Ciência e Tecnologia do Ceará, Av. 13 de Maio, 2081, Benfica, 60040-531 Fortaleza, Ceará, Brazil
[c] Departamento de Física, Universidade Federal do Ceará, Centro de Ciências, Caixa Postal 6030, Campus do Pici, 60455-760 Fortaleza, Ceará, Brazil

ARTICLE INFO

Article history:
Received 13 June 2009
Received in revised form
13 November 2009
Accepted 30 November 2009
Available online 11 December 2009

Keywords:
Orthorhombic $CdGeO_3$
Structural properties
Band structure
Effective masses
Optical absorption
Dielectric function

ABSTRACT

Orthorhombic perovskite $CdGeO_3$ was studied using the density-functional theory (DFT) formalism. The electronic band structure, density of states, effective masses, dielectric function and optical absorption were obtained. Comparing with orthorhombic $CaGeO_3$, which is an indirect $S \rightarrow \Gamma$ gap material, the substitution of calcium by cadmium changes the valence band maximum from the S point to the Γ point in reciprocal space, and decreases the Kohn–Sham band gap energy. Our results suggest that orthorhombic $CdGeO_3$ has features of a semiconductor and is potentially useful for optoelectronic applications.

1. Introduction

When synthesized under ambient pressure, cadmium germanate ($CdGeO_3$) exhibits a complex structure resembling the pyroxenoids. In one paper published two decades ago, Susaki [1] obtained four $CdGeO_3$ polymorphs in the temperature range from 600 to 1200 °C and varying pressure up to 12 GPa. As the pressure increases, the pyroxenoid phase ($CdGeO_3$ I) is transformed successively into garnet ($CdGeO_3$ II), ilmenite ($CdGeO_3$ III, hexagonal) and perovskite ($CdGeO_3$ IV, orthorhombic). Structural refinement of the $CdGeO_3$ IV single crystal showed that this structure is isomorphic to $GdFeO_3$ with symmetry space group *Pbnm*. $CdGeO_3$ I transforms into the distorted garnet $CdGeO_3$ II (tetragonal symmetry) at about 1 GPa and 973 K; the distorted perovskite phase ($CdGeO_3$ IV) forms at 13 GPa and 1173 K [2], remaining stable even at 110 GPa and 2000 K [3]. The ilmenite ($CdGeO_3$ III) phase was shown to exist between the stability fields of the garnet and the distorted perovskite phase [2]. Since $CdGeO_3$ can be quenched to ambient condition, it has being mainly studied, together with $CaGeO_3$, $CaSiO_3$, $MgSiO_3$ and other ABO_3 structures, to understand the mechanisms that lead to the stabilization of the various perovskite crystals, a long standing problem in materials science [4].

On the other hand, considering the interest in the $CaXO_3$ (X = C, Si, Ge, Sn, Pb) class of materials, first principles calculations of the structural, electronic, and optical properties were performed by our research group for all the $CaCO_3$ polymorphs (calcite [5], aragonite [6], and vaterite [7]), for triclinic $CaSiO_3$ [8], orthorhombic $CaGeO_3$ [9], $CaSnO_3$ [10], and $CaPbO_3$ [11]. The calculated band structures suggest an overall trend of the minimal band gap energy to decrease, with some oscillation, according to the sequence $CaCO_3$ calcite ($\approx$5.0 eV)–$CaSiO_3$($\approx$5.4 eV)–$CaGeO_3$($\approx$2.3 eV)–$CaSnO_3$($\approx$2.9 eV)–$CaPbO_3$ ($\approx$0.94 eV).

Recently, our group begun to study the electronic properties of $CdXO_3$ (X = C, Si, Ge, Sn, Pb) crystals using the density functional theory (DFT) formalism considering both the local density and generalized gradient approximations, LDA and GGA, respectively [12]. It was demonstrated that hexagonal $CdCO_3$ and triclinic $CdSiO_3$ have indirect main energy band gaps, while orthorhombic $CdGeO_3$ and $CdSnO_3$ exhibit direct interband transitions. Orthorhombic $CdPbO_3$ has a very small indirect band gap. The Kohn–Sham minimum electronic band gap oscillates as a function of the X ns level, changing from 2.94 eV (hexagonal $CdCO_3$, LDA) to 0.012 eV (orthorhombic $CdPbO_3$, LDA). In order to perform a meaningful comparison between the properties of $CaXO_3$ and

* Corresponding author. Fax: +55 85 3307 3711.
E-mail address: ewcaetano@gmail.com (E.W.S. Caetano).

0022-4596/$ - see front matter © 2009 Elsevier Inc. All rights reserved.
doi:10.1016/j.jssc.2009.11.033

$CdXO_3$, we have considered the orthorhombic phases for $CdGeO_3$, $CdSnO_3$, and $CdPbO_3$ since orthorhombic $CaGeO_3$, $CaSnO_3$, and $CaPbO_3$ were considered early [9–11].

Orthorhombic calcium germanate, $CaGeO_3$, is an analogue of $CdGeO_3$ IV whose electronic band structure, density of states, dielectric function and optical absorption was studied recently using density-functional theory (DFT) considering both the local density and generalized gradient approximations, LDA and GGA, respectively [9]. Two very close indirect ($S \rightarrow \Gamma$) and direct ($\Gamma \rightarrow \Gamma$) band gap energies of 1.68 eV (2.31 eV) and 1.75 eV (2.41 eV) were obtained for $CaGeO_3$ within GGA (LDA), as well as effective masses for electrons and holes. The substitution of carbon by germanium changes the localization of the valence band maximum of the indirect transition, and leads to a decrease of almost 2.0 eV in the Kohn–Sham band gap energies when one compares both the orthorhombic $CaGeO_3$ and $CaCO_3$ (aragonite) band structures. The calculated dielectric functions of orthorhombic $CaGeO_3$ for incident light polarized along the 1 0 0, 0 1 0, and 0 0 1 crystalline directions look very similar to each other, but for the 1 1 1 direction the optical response is stronger due to the partial alignment of some Ca–O electric dipoles with the 1 1 1 polarized electric field. In the energy range between 2.3 and 7.0 eV, approximately, optical absorption increases slowly, but from 7.0 eV to larger energies, optical absorption increases more quickly due to the appearance of transitions involving valence states with strong O-2*p* contributions and Ca-2*s* conduction states for energies larger than 7.0 eV.

The most important feature of the series of papers we are publishing in $CaXO_3$ and $CdXO_3$ ($X = C$, Si, Ge, Sn, Pb) is to allow a comparative study of these crystals with focus on their electronic and optical properties. First-principles calculations of the structure of $CdGeO_3$ under high pressures have been performed recently [13] using a GGA exchange-correlation functional, but after an extensive research in the literature we have not found any report on the electronic and optical properties of orthorhombic $CdGeO_3$. Thus the focus of this work is to simulate the structural and optoelectronic properties of calcium germanate by applying quantum first-principles calculations using the density functional theory (DFT) formalism. A comparison with corresponding results for $CaGeO_3$ orthorhombic is also performed, showing how the replacement of Ca (Pauling ionic radius 0.99 Å) with Cd (Pauling ionic radius 0.97 Å) modifies the electronic band structures and partial densities of states, as well as their optical properties.

2. Methodology

All calculations here use crystallographic data obtained from Susaki's paper [1] for $CdGeO_3$ IV, which has a structure very similar to that of orthorhombic $CaGeO_3$, whose electronic and structural properties we investigated previously [9]. Our main motivation for this work is to study how switching from Ca to Cd, within the same crystalline phase, changes the unit cell geometry and the electronic features of these materials. $CdGeO_3$ IV has an orthorhombic unit cell with lattice parameters $a = 5.2114(7)$ Å, $b = 5.2608(6)$ Å, and $c = 7.44263(7)$ Å, space group *Pbnm* (62), and $Z = 4$. Each germanium atom is connected to six oxygen atoms and each cadmium atom has its closest neighborhood formed by four oxygen atoms, creating a tridimensional array of GeO_6 tilted octahedra and CdO_4 distorted tetrahedra (see Fig. 1).

For the first principles calculations we have used the CASTEP code [14], which implements the density functional theory (DFT) formalism [15,16] using a plane wave basis set and pseudopotentials to represent the core electrons. Taking into account the limitations of the local density approximation (LDA) for the exchange-correlation energy [16–18], we have used both the LDA and the generalized gradient approximation (GGA) exchange-correlation functionals [19,20]. The standard LDA exchange-correlation functional of Perdew and Ceperley [21,22] and the GGA exchange-correlation functional of Perdew–Burke–Ernzerhof (PBE) [23] were chosen. In general, DFT results for bulk materials using the PBE exchange-correlation energy are similar to the ones obtained using the well established PW91 functional [24]. In order to optimize the geometry of the $CdGeO_3$ unit cell, ultrasoft Vanderbilt-type pseudopotentials [25] were employed with the following valence configurations: Cd $4d^{10}$ $5s^2$, Ge $4s^2$ $4p^2$, and O $2s^2$ $2p^4$, so each unit cell has 136 electrons. These ultrasoft pseudopotentials contribute to decrease the computational costs associated with typical DFT runs using a plane wave basis set because their smoothness allows one to choose a smaller energy cutoff. To evaluate integrals in reciprocal space, a Monkhorst–Pack $6 \times 6 \times 4$ sampling was adopted [26]. This grid size was chosen to ensure that both the geometry and electronic band structure are well converged.

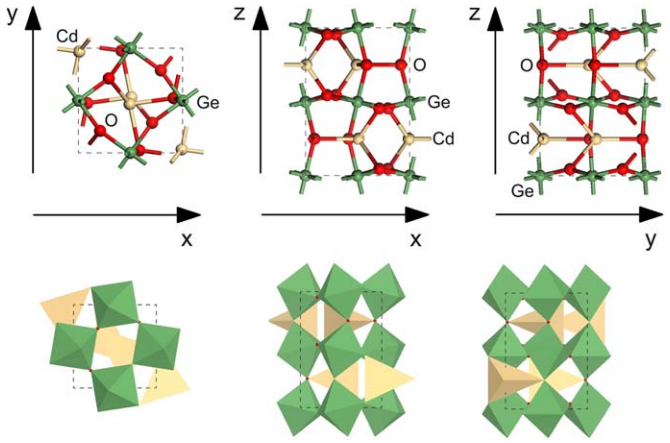

Fig. 1. Different views of the $CdGeO_3$ IV unit cell. Top: atoms and internal bonding. The arrows point along the main crystal directions. Bottom: GeO_6 tilted octahedra and CdO_4 tetrahedra forming the orthorhombic phase.

In the geometry optimization scheme, both the lattice parameters and internal atomic positions are modified to find a total energy minimum for the $CdGeO_3$ unit cell. The convergence thresholds selected for all geometry optimizations were: total energy variation smaller than 0.5×10^{-5} eV/atom, maximum force smaller than 0.01 eV/Å, maximum displacement smaller than 0.5×10^{-3} Å, and maximum stress component smaller than 0.02 GPa. The convergence tolerance window was of two steps, and the optimization method used the BFGS minimizer [27]. The basis set quality is kept fixed while the unit cell volume changes. Each self-consistent field step was carried out with tolerances of 0.5×10^{-6} eV for the total energy variation and 0.1389×10^{-6} eV for the electronic eigenenergies. The plane wave basis set energy cutoff was chosen to be 500 eV and the density of charge was calculated using an energy cutoff of 1500 eV.

After the geometry optimization, the electronic band structure and partial density of states were calculated. Optical properties were also obtained after a single point energy run using norm-conserved pseudopotentials [28] with a plane wave basis set energy cutoff of 700 eV (the CASTEP code is unable to obtain these properties using ultrasoft pseudopotentials). Electron and hole effective masses at the band structure extrema were found through parabolic fitting as described in Ref. [9].

3. Results and discussion

3.1. Geometry optimization

In Table 1 one can see the lattice parameters and unit cell volumes for $CdGeO_3$ IV obtained from our DFT calculations, as well as the experimental values from Ref. [1]. The estimates for *a*, *b* and *c* using the LDA exchange-correlation functional are smaller than the X-ray data by -1.5% at most (for *c*), and the unit cell volume is smaller by -3.7%. The GGA lengths for the lattice parameters are larger than experimental lengths by 2.0% at most (*a* and *b*) and the predicted GGA unit cell volume is 6.0% larger than the experimental value. These differences are well within the typical margin of 2.0% for well converged DFT optimized structures. Lattice parameters obtained using the GGA exchange-correlation energy are in general bigger than experimental data [19,20], while the LDA exchange-correlation energy tends to overestimate the interactions between atoms producing smaller unit cells. The average pressure on the unit cell after the GGA (LDA) computation was 0.0079 GPa (-0.0035 GPa), and the components of the symmetrized stress tensor were $\varepsilon_{xx} =$ -0.007357 GPa (0.008019 GPa), $\varepsilon_{yy} =$ -0.002212 GPa (0.009875 GPa), and $\varepsilon_{zz} =$ -0.014125 GPa (-0.007519 GPa), with hydrostatic stress.

As expected, both theoretical and experimental unit cell figures for $CdGeO_3$ IV and orthorhombic $CaGeO_3$ are very close due to the similar ionic radii of Ca and Cd. The $CaGeO_3$ unit cell volume from experiment is only 1.1% larger than the corresponding $CdGeO_3$ IV value, and the lattice parameter differences are 0.94% (*a*), 0.15% (*b*), and 0.03% (*c*). For the LDA data we have the unit cell volume of $CaGeO_3$ a bit smaller (-0.4%) than the volume of $CdGeO_3$ IV. Nevertheless, the parameter *a* for $CaGeO_3$ is slimly larger (0.2%) than for cadmium germanate. For the GGA results, the $CaGeO_3$ unit cell volume is 0.2% smaller than the $CdGeO_3$ unit cell. So one can conclude that both methods, LDA and GGA, within the convergence levels found adequate, tend to overestimate by a small amount the binding strength of Cd when this atom replaces Ca in an oxygen neighborhood. Indeed, the LDA Cd–O smallest interatomic distance is 2.19 Å, while for Ca–O the respective value is 2.28 Å. The GGA figures for the same distances are 2.25 Å (Cd–O) and 2.33 Å (Ca–O).

The O–Ge–O angles within each GeO_6 octahedra, according with the GGA computations, vary from 88.44° to 91.56° (the experimental range is 88.67−91.33°, and the LDA range is 88.72−91.28°), while the Ge–O–Ge angle which measures the octahedra tilting is 150.5° (the experimental value is 151.8°, and the LDA angle is 152.9°). The O–Cd–O angles vary from 84.54° to 131.7° (experimental: 85.27−130.8°; LDA: 85.06−130.9°). In general, the LDA calculation leads to better predictions for the structural parameters in comparison with the X-ray measurements.

Table 1
LDA and GGA lattice parameters (in Å) of $CdGeO_3$ IV and $CaGeO_3$ orthorhombic.

	LDA	GGA	Exp.
$CdGeO_3$			
a	5.152(-1.1%)	5.316(+2.0%)	5.2114(7)
b	5.197(-1.2%)	5.369(+2.0%)	5.2608(6)
c	7.334(-1.5%)	7.579(+1.8%)	7.44263(7)
$V = abc$	196.4(-3.7%)	216.3(+6.0%)	204.05(3)
$CaGeO_3$			
a	5.162(-1.9%)	5.32(+1.1%)	5.2607
b	5.183(-1.6%)	5.37(+2.0%)	5.2688
c	7.309(-1.8%)	7.54(+1.3%)	7.4452
$V = abc$	195.6(-5.2%)	215.8(+4.6%)	206.36

The unit cell volumes (in $Å^3$) are also shown. Percentages indicate the difference between the calculated values and the experimental data from Ref. [1] for $CdGeO_3$ IV, and Ref. [29] in the case of orthorhombic $CaGeO_3$. Theoretical values for orthorhombic $CaGeO_3$ were obtained from our previous work [9].

3.2. Electronic structure

Fig. 2 presents the Kohn–Sham band structure of $CdGeO_3$ IV with the partial density of states per orbital, as well as a picture of the first Brillouin zone for guidance. The orthorhombic phase of cadmium germanate exhibits (see Fig. 2, top-left), according with the GGA calculations, a set of twelve bands between -19 and -12 eV, with dominant *s* character, a set of four *s* bands between -10 and -7 eV, and a dense set of 20 *d* bands between -7 and -6 eV. The top of the valence band (VB) has a dominant *p* character, with 32 bands between -5 and 0 eV (the energy of the highest valence electronic eigenstate was chosen to be zero). The valence band starts from approximately 1 eV, with six *s* bands in the energy range between 1 and 6 eV and six *p* bands between 6 eV and about 9 eV. The LDA results are in general similar, but with the conduction band minimum shifted by about 1 eV above the GGA value.

As one can see from the bottom-left of Fig. 2, $CdGeO_3$ IV has a direct ($\Gamma \rightarrow \Gamma$) band gap in both GGA and LDA computations, being 0.82 eV (GGA) and 1.67 eV (LDA). The closest indirect band gap involving the valence band maximum and a conduction band minimum occurs between the Γ (valence band) and *Y* points, and is 3.28 eV (GGA) or 4.08 eV (LDA). Contrasting the GGA band structures of $CdGeO_3$ IV and orthorhombic $CaGeO_3$ [9], depicted near its band gap at the bottom-right part of Fig. 2, we note that $CaGeO_3$ has an indirect main band gap between the valence band maximum at the *S* point and the conduction band minimum at Γ of 1.68 eV, while the direct $\Gamma \rightarrow \Gamma$ energy transition is 1.75 eV. The uppermost valence bands of orthorhombic $CaGeO_3$ are very distinct from the corresponding ones for $CdGeO_3$ IV. At the *S* point, for example, the uppermost VB of $CdGeO_3$ IV has a minimum, while for $CaGeO_3$ the same point is the VB maximum. The uppermost VB along the Γ−Z−T−Y−S path presents a consistent decrease in energy for $CdGeO_3$, while the same curve for orthorhombic $CaGeO_3$ increases in energy. In general, the VB minima of orthorhombic $CaGeO_3$ are higher in energy when compared with the $CdGeO_3$ IV values. On the other hand, the conduction bands (CBs) of both crystals, $CdGeO_3$ IV and orthorhombic $CaGeO_3$, look very similar, the main differences between them arising from the distinct values of the energy band minimum at the Γ point and the smoother curvature for the $CaGeO_3$ CB at Γ, which leads to larger electron effective masses for this material in comparison with $CdGeO_3$ IV (see more comments on effective masses below).

A statistical comparison between the GGA and LDA curves for the lowest conduction band of $CdGeO_3$ IV reveals that the LDA curve is, on average, 0.8344 eV above the GGA curve, with a standard deviation of 0.2426 eV and mean absolute deviation of 0.1824 eV. Having said that, some discretion is advised when dealing with energy band gaps predicted by DFT calculations. It is well known that Kohn–Sham eigenvalues cannot be equated to the correct excitation energies [30]. In fact, to estimate energy band gaps one must know the exact non-analytic form for the exchange-correlation energy, as indicated in Ref. [31]. Because the exact exchange-correlation functional is unknown, approximations such as LDA and GGA systematically lead to wrong results for energy gaps in semiconductors and insulators. The general trend is for LDA to underestimate the main gap of these materials by about 40%, with the GGA trend being even worse. Despite this problem, some reports point that a rigid shift in the LDA

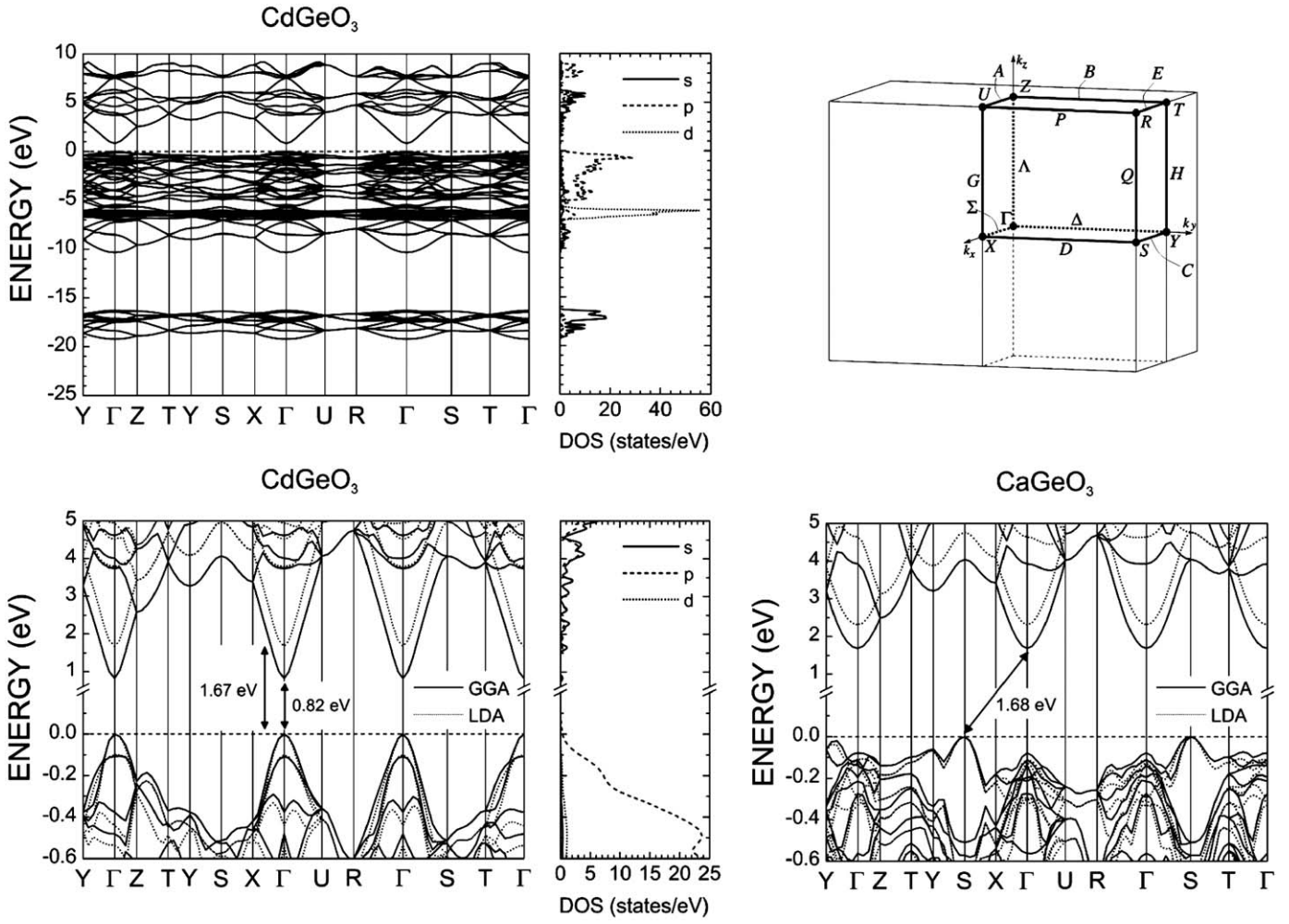

Fig. 2. Electronic Kohn–Sham band structure of $CdGeO_3$ IV. Top, right: Brillouin zone with high symmetry points and directions assigned. Top, left: full Kohn–Sham GGA band structure obtained from our first principles calculations. Bottom, left (right): close-up of both GGA and LDA band structures of $CdGeO_3$ IV (orthorhombic $CaGeO_3$) with their main energy band gaps indicated. Partial density of states (GGA) curves for the $CdGeO_3$ IV bands are also shown.

conduction bands is enough to produce a reasonable agreement with the more sophisticated (and much more expensive in computational terms) quasi-particle GW approximation, which is able to predict optical excitation frequencies in semiconductors within 0.1 eV [30,32–34]. For results obtained in a way analogue to our work, one can look into the work of Migas et al. [35] on the electronic structure and dielectric functions of Ca_2X (X = Si,Ge,Sn,Pb) compounds. Lebègue et al. [36] obtained the electronic properties of Ca_2Si using the GW approximation for the orthorhombic and cubic phases, finding, as one could expect, valence and conduction eigenenergies very different from the results obtained using DFT. Recent results for the $BaTiO_3$ ferroelectric oxide reinforce the belief that a rigid shift of the LDA valence band and conduction band energies is enough to reach a good agreement with the GW method [37]. As the GGA band structure presented here looks very similar to the LDA one, we think that our analysis is valid if we keep in mind the need to increase the GGA band gaps by a few eV to achieve an agreement with the true $CdGeO_3$ band gap. From this discussion, we can also presume that the main direct energy gap of $CdGeO_3$ IV is about 1 eV smaller than the indirect gap of orthorhombic $CaGeO_3$, as relative energies of similar materials using the same methodology of calculation should suffer less from the DFT gap problem. To the knowledge of the authors, however, there is no experimental measurement of the energy gap of $CdGeO_3$IV reported in the literature.

A detailed plot of the partial density of states (PDOS) of $CdGeO_3$ IV per atomic species per orbital is shown in the left side of Fig. 3, with the equivalent PDOS for orthorhombic $CaGeO_3$ shown in the right side. At the top-left, one can see the contribution to the electronic structure from the Cd atoms. Its most important feature is the presence of a sharp peak with height of 14 states/eV at about -6.3 eV arising from the Cd 4*d* orbitals. Smaller peaks in the 4.5−6.2 eV range in the conduction band stem from the Cd 5*s* levels and reach a maximum PDOS value of about 2 states/eV. In the 7.5–9.0 eV energy interval some peaks are present related to unoccupied Cd 6*p* states, with maximum of about 1 state/eV. In contrast, the Ca share to the PDOS of orthorhombic $CaGeO_3$ exhibits a 3*p* peak around -18 eV and a barely visible Ca 4*s* peak at about 8 eV [9]. There are also deep valence states originated from Ca 3*s* (a very sharp peak at about -37 eV related to a flat, atomic-like energy band, not shown in Fig. 3) orbitals.

PDOS contributions from Ge, on the other hand, are broader and tend to be smaller in comparison with Cd due to the fact that only four electrons in its outermost shell were explicitly taken into account during the calculations (for Cd, the number of electrons explicitly considered was 12). Ge contributions to PDOS

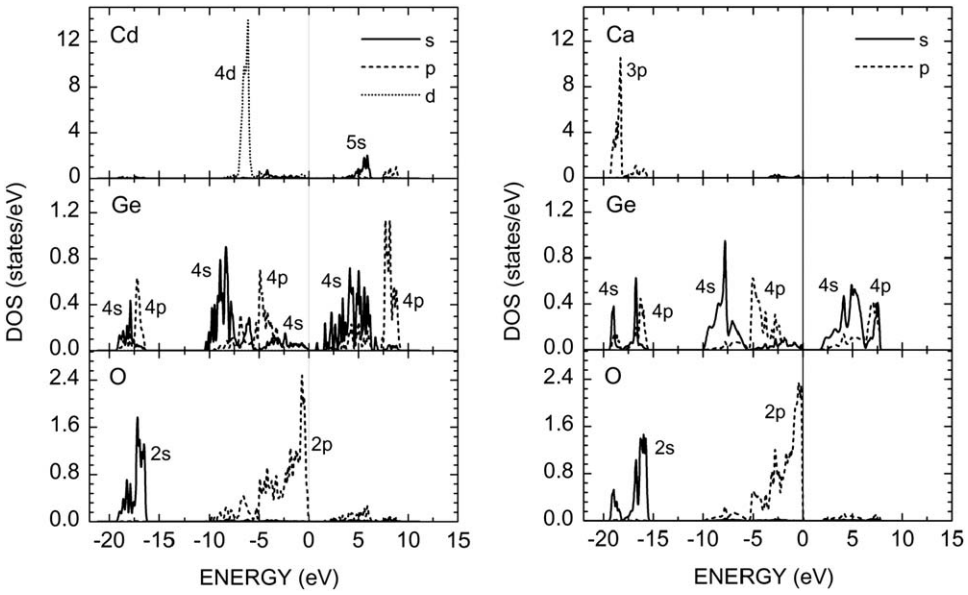

Fig. 3. Left (right): GGA partial density of states of $CdGeO_3$ IV (orthorhombic $CaGeO_3$) for each atomic species. The vertical line indicates the top of the valence band.

have a pattern of alternating *s* and *p* dominating bands in the energy intervals -19 to -17.5 eV (*s*), -17.5 to -16.2 eV (*p*), -10.4 to -7.3 eV (*s*), -7.3 to -6.4 eV (*p*), -6.4 to -5.6 eV (*s*), -5.6 to -3.5 eV (*p*), and -3.5 to 0 eV (*s*). For the conduction band, the Ge 4*s* orbitals dominate the PDOS in the 0.8–7.3 eV energy range, while for the 7.3–9.5 eV energy range the PDOS dominant contribution stems from Ge 4p orbitals. Similar features are observed for orthorhombic $CaGeO_3$ (Fig. 3, right), with a significant difference for the Ge 4*p* conduction bands in the 8–9 eV, where the $CdGeO_3$ crystal has a stronger contribution from these orbitals while the $CaGeO_3$ corresponding bands have a mixed Ge 4*s*–4*p* character. Finally, the six electrons in the valence shell of each oxygen atom produce two sets of valence bands, one of O 2*s* character comprising energies from -19 to -16 eV, and the other, very broad, with O 2*p* character ranging from -10 to 0 eV and with a maximum of 2.5 states/eV close to 0 eV. There are small O-2*p* contributions for the conduction bands in the energy interval 1.7–6.3 eV. As a matter of fact, one can say that the top of the valence band of $CdGeO_3$ IV is ruled by O 2*p* contributions, while the bottom of the conduction band is formed mainly from Ge 4*s* orbitals (0.8–5.0 eV) and Cd 5*s* (5.0–6.2 eV), with a single PDOS peak from Ge 4*s* at 0.8 eV (the main band gap of $CdGeO_3$ IV) with height of 0.1 state/eV approximately. The oxygen PDOS for orthorhombic $CaGeO_3$ looks very similar to the $CdGeO_3$ IV oxygen PDOS.

The concept of an effective mass is very useful in the study of solids. The transport of charge carriers can be modeled using a quasi-newtonian approximation in which electrons in the conduction band and holes in the valence respond to external electromagnetic fields as particles with a mass dependent on the direction they are moving inside the material. Effective masses can be obtained from the electronic band structure by considering the band curves passing through high symmetry points in the Brillouin zone and measuring their curvature, a procedure we have explained with details in a previous work [9]. Larger effective masses mean that the band curves have less curvature, while smaller effective masses mean highly curved bands. A single effective mass is calculated for each band curve starting from a high symmetry point to another. In this work we obtained the effective masses for holes and electrons along directions with origin at the Γ point for the valence and conduction band extrema. The results we obtained are summarized in Table 2.

Table 2
Effective masses for holes and electrons (in m_0 units) in $CdGeO_3$ IV along a set of high symmetry directions starting at the Γ point.

Direction	Hole mass		Electron mass	
	LDA	GGA	LDA	GGA
$\Gamma \rightarrow S$	0.580	0.607	0.095	0.074
$\Gamma \rightarrow Z$	3.977	10.97	0.305	0.351
$\Gamma \rightarrow R$	0.529	0.572	0.076	0.059
$\Gamma \rightarrow U$	1.042	1.209	0.119	0.091
$\Gamma \rightarrow T$	0.807	0.861	0.121	0.093
$\Gamma \rightarrow Y$	1.120	1.162	0.212	0.170

m_0 is the free electron mass.

The GGA and LDA effective masses are somewhat close, with GGA hole masses being larger in comparison with LDA for holes and smaller (except along the $\Gamma \rightarrow Z$ direction) for electrons. The valence band curve with the heaviest hole connects the Γ and Z points to each other, $m_h(\Gamma \rightarrow Z, \mathrm{LDA}) = 3.997$ and $m_h(\Gamma \rightarrow Z, \mathrm{GGA}) = 10.97$. Hole and electron effective masses along the $\Gamma \rightarrow S$ and $\Gamma \rightarrow R$ lines are comparable, as well as hole masses along the $\Gamma \rightarrow U$ and $\Gamma \rightarrow Y$ lines. A general trend one can easily observe is that holes are heavier than electrons along the same direction. The degree of anisotropy for all effective masses is pronounced, indicating that the transport of carriers inside the $CdGeO_3$ IV crystal under electric or magnetic fields is highly dependent on the direction of the external field relative to the crystal axes. An anisotropic set of effective masses was also found for orthorhombic $CaGeO_3$ [9], with very large hole effective masses along lines starting from the *S* point to the *R*, *U*, *T* and *Y* points in the Brillouin zone. Effective masses of electrons in orthorhombic $CaGeO_3$ along the same directions we present in Table 2 are more isotropic, with average of 0.40 and standard deviation of 0.033 free electron mass for the LDA results and average of 0.45 and standard deviation of 0.044 free electron mass for the GGA results. In comparison, the same figures for $CdGeO_3$ IV are: average electron mass of 0.15 and standard deviation of 0.08 free electron mass (LDA) and average electron mass of 0.14 and standard deviation of 0.11 free electron mass (GGA). Considering that the electron effective masses of $CdGeO_3$ IV are smaller in comparison with orthorhombic $CaGeO_3$, and that the main band gap of the first is direct and about 1 eV

smaller than the second, one can expect that $CdGeO_3$ IV has better electrical conductivity than $CaGeO_3$ and could be used for optoelectronic applications.

3.3. Optical properties

The static dielectric constant of a material, being a ground state feature, does not require quasi-particle rectifications. The dielectric function $\varepsilon(\mathbf{r}, \mathbf{r}', \omega)$, however, changes when one includes the self-energy correction and local field effects. Beyond that, excitonic effects cannot be incorporated in the dielectric function due to limits in the computational methods currently available [38]. Thus the results here presented for $CdGeO_3$, like the results for the electronic band structure, must be viewed with care. Our limited computational resources have not allowed us to pursue quasiparticle corrections, and the dielectric function curves are only zero order approximations. Notwithstanding such restriction, we mention here the work by Lebègue et al. [36], which shows that LDA dielectric functions are in general resized, but with an energy shift not very pronounced, when local-field features are taken into account. So again we hope that the results here presented on the dielectric function and optical absorption are valuable for experimental studies of the optical properties of $CdGeO_3$ IV. Indeed, the dielectric function of perovskite $CaTiO_3$ was calculated using an approach very alike to ours [39]. The way the dielectric function is calculated here is the same used in Ref. [9], with the real part of the dielectric function obtained from the imaginary part through the Kramers–Kronig relationship [40,41].

In Fig. 4 we present the real (top) and imaginary (middle) parts of the complex dielectric function ε of $CdGeO_3$ IV, and its optical absorption (bottom), calculated within the GGA approximation. Optical properties for light strucking a polycrystalline sample, and for light rays polarized along a set of crystalline planes, 1 0 0, 0 1 0, 0 0 1, and 1 1 1 were simulated. As observed for $CaGeO_3$ [9], the Re(ε) and Im(ε) curves for light polarized along the 1 0 0, 0 1 0, and 0 0 1 planes behave likewise, while the dielectric function components for the 1 1 1 direction have more pronounced maxima and minima. One can suppose that the cause is similar: in $CaGeO_3$, the alignment of Ca–O dipoles with the electric field polarized along 1 1 1; in $CdGeO_3$ IV, an analogous situation involving Cd–O dipoles. The static dielectric constant (electronic contribution only) of $CdGeO_3$ for a polycrystalline sample is 6.29. In the case of light with polarization along the 1 0 0, 0 1 0, and 0 0 1 directions, $\varepsilon(\omega = 0)$ varies between 4.55 (001) and 5.00 (100), and for the 1 1 1 direction, $\varepsilon(\omega = 0) = 12.3$. Maxima of Re($\varepsilon$) for a polycrystalline sample occur at 1.30, 2.02, 2.45, 2.79, 3.13, 3.36, 3.60, 3.91, and 4.10 eV, and from 8.01 to 16.4 eV, Re(ε) < 0. The optical absorption is closely related to the imaginary part of ε, thus we now look to the optical absorption instead of commenting on Im(ε). At the bottom part of Fig. 4, a close-up of the optical absorption in the 0–5 eV energy range is shown. As occurred for the dielectric function, the optical absorption peaks are more intense for light polarized along the 1 1 1 crystal plane, and the curves for the 1 0 0, 0 1 0, 0 0 1 cases are very close. The firstabsorption peak in the case of a polycrystalline sample appears at 1.2 eV, and is very small. The first pronounced peak in this case occurs at 1.4 eV, related to transitions involving valence states with dominant O 2*p* character to Ge 4*s* conduction states. There is an optical absorption gap between 1.6 and 2.0 eV followed by four peaks with almost the same height at 2.2, 2.6, 2.8, and 2.9 eV. For energies above 3.0 eV, the optical absorption tends to increase rapidly, with the emergence of transitions involving O 2*p* valence bands and Cd 5*s* conduction bands.

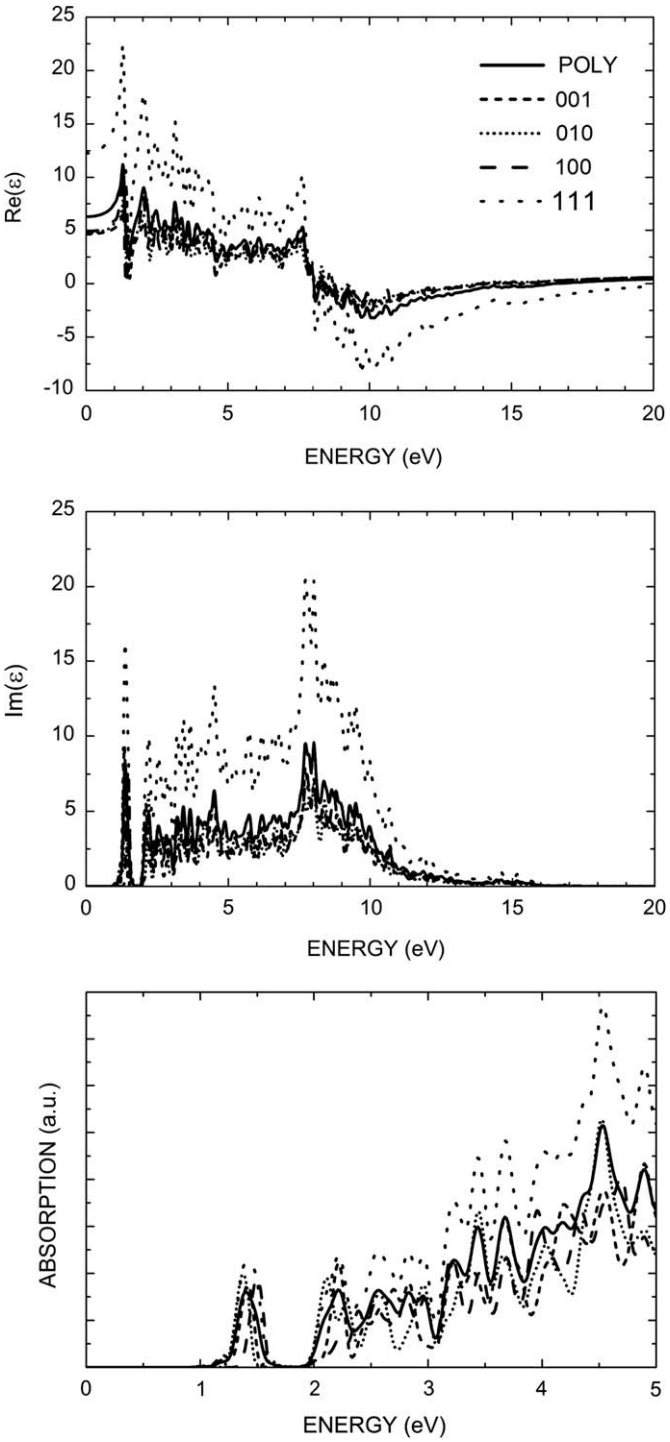

Fig. 4. Complex dielectric function ε: real (top) and imaginary (middle) components. Bottom: optical absorption. Curves for a polycrystalline sample (POLY) and for incident light with polarization planes aligned to some crystalline axes are shown.

4. Conclusions

In summary, we have presented the results of quantum first principles calculations within the density functional formalism for que geometry optimization, band structure, density of states and optical properties (dielectric function and optical absorption) of orthorhombic $CdGeO_3$ ($CdGeO_3$ IV), contrasting these results with similar data obtained for orthorhombic $CaGeO_3$ [9]. Using

the local density and generalized gradient approximations (LDA and GGA, respectively) for the exchange-correlation functionals, we have obtained lattice parameters that compare well with experimental X-ray data, with the difference between calculated values and experiment being less than or equal to 2%. The range of variation for the O–Ge–O angles in the GGA (LDA) approach is larger (smaller) than the measured one because the GGA (LDA) exchange-correlation energy tends to produce smaller (larger) forces between atoms, an effect also responsible for the large (small) lattice parameters predicted by using this level of theory in comparison with measurements. Both methods, LDA and GGA, slightly overestimate the intensity of the Cd–O interaction in comparison with the Ca–O interaction in $CaGeO_3$ orthorhombic, so the LDA and GGA volumes for the $CdGeO_3$ unit cell, $V_{LDA}(CdGeO_3)$ and $V_{GGA}(CdGeO_3)$, respectively, are larger than the corresponding $V_{LDA}(CaGeO_3)$ and $V_{GGA}(CaGeO_3)$ values, a behavior that opposes the experimental fact that the $CdGeO_3$ unit cell volume is the smallest one, $V_{Exp.}(CdGeO_3) < V_{Exp.}(CaGeO_3)$. The Kohn–Sham band structure of $CdGeO_3$ IV reveals that this material has a direct band gap, differing from $CaGeO_3$, which has an indirect band gap from the S point in the valence band to the Γ point in the conduction band. The GGA band gap of $CdGeO_3$ IV is 0.82 eV while the LDA band gap is 1.67 eV. As the DFT approach tends to underestimate the band gap of semiconductors and insulators, one can expect that the band gap of $CdGeO_3$ IV is larger than 1.67 eV, being probably larger than 2.7 eV considering the typical error margin of DFT computations. The indirect energy band gaps (LDA and GGA) of orthorhombic $CaGeO_3$ in comparison are about 1 eV larger than the $CdGeO_3$ IV figures. A sharp Cd 4*d* energy band appears atabout 6.3 eV below the valence band maximum, and the top of the valence band is formed from states with strong O 2*p* character. The bottom of the conduction band originates mainly from Ge 4*s* states. Effective masses (all values measured in units of the free electron mass) for electrons and holes in $CdGeO_3$ IV are very anisotropic, like effective masses in orthorhombic $CaGeO_3$, with heaviest holes along the $\Gamma \rightarrow Z$ direction (LDA and GGA masses approximately 4.0 and 11, in this order). Despite that, for the most part of all directions within the Brillouin zone we investigated we have found electron masses smaller than 0.36 and hole masses smaller than 1.3, which suggests, if we consider a possible direct band gap of about 3 eV, that $CdGeO_3$ IV could behave under some circumstances as a wide band gap semiconductor with potential for optoelectronic applications (for example, doped $CdSiO_3$, a "relative" of $CdGeO_3$, is used as a host material for long lasting phosphorescence devices [42–44]). The GGA dielectric function curves (real and imaginary parts) of $CdGeO_3$ IV when the polarization plane is aligned with the 1 0 0, 0 1 0, and 0 0 1 crystal planes are almost identical. When the polarization plane is the 1 1 1 crystal plane, however, the maxima and minima of the dielectric function components are more pronounced than the 1 0 0, 0 1 0, 0 0 1 cases due to the alignment of Cd–O dipoles with the electric field, as appears to happen with orthorhombic $CaGeO_3$ [9]. The GGA dielectric constant of $CdGeO_3$ IV for a polycrystalline sample (taking into account only the electronic contribution) is 6.29, and the optical absorption has its first pronounced peak at 1.4 eV related to optical transitions from valence states with dominant O 2*p* character at the top of the valence band to conduction states stemming mainly from Ge 4*s* orbitals. Above 3.0 eV, the absorption of light tends to increase with the emergence of transitions from the O 2*p* valence bands to Cd 5*s*-related conduction bands. Finally, one can also argue that the existence of the orthorhombic $CdGeO_3$ phase at high temperature and pressure suggest promising applications of this semiconductor in harsh environmental conditions.

Acknowledgments

V.N.F., J.A.P.C., and E.L.A. are senior researchers from the Brazilian National Research Council CNPq, and would like to acknowledge the financial support received during the development of this work from the grants CNPq-CTENERG 504801/2004-0 and CNPq-Rede NanoBioestruturas 555183/2005-0. J.M.H. was sponsored by a graduate fellowship from the Brazilian National Research Council (CNPq) at the Physics Department of the Universidade Federal do Rio Grande do Norte. E.W.S.C. received financial support from CNPq-process number 304338/2007-9.

References

[1] J.-I. Susaki, Phys. Chem. Miner. 16 (1989) 634.
[2] M. Akaogi, A. Navrotsky, Phys. Chem. Miner. 14 (1987) 435.
[3] S. Tateno, K. Hirose, N. Sata, Y. Ohishi, Phys. Chem. Miner. 32 (2006) 721.
[4] B. Magyari-Köpe, L. Vitos, B. Johansson, J. Kollár, Phys. Rev. B 66 (2002) 092103.
[5] S.K. Medeiros, E.L. Albuquerque, F.F. Maia Jr., E.W.S. Caetano, V.N. Freire, J. Phys. D Appl. Phys. 40 (2007) 5747.
[6] S.K. Medeiros, E.L. Albuquerque, F.F. Maia Jr., E.W.S. Caetano, V.N. Freire, Chem. Phys. Lett. 430 (2006) 293.
[7] S.K. Medeiros, E.L. Albuquerque, F.F. Maia Jr., E.W.S. Caetano, V.N. Freire, Chem. Phys. Lett. 435 (2007) 59.
[8] J.M. Henriques, E.W.S. Caetano, V.N. Freire, J.A.P. da Costa, E.L. Albuquerque, Chem. Phys. Lett. 427 (2006) 113.
[9] J.M. Henriques, E.W.S. Caetano, V.N. Freire, J.A.P. da Costa, E.L. Albuquerque, J. Solid State Chem. 180 (2007) 974.
[10] J.M. Henriques, E.W.S. Caetano, V.N. Freire, J.A.P. da Costa, E.L. Albuquerque, J. Phys. Condens. Matter 19 (2007) 106214.
[11] J.M. Henriques, C.A. Barboza, E.L. Albuquerque, E.W.S. Caetano, V.N. Freire, J.A.P. da Costa, J. Phys. D Appl. Phys. 41 (2008) 065405.
[12] C.A. Barboza, J.M. Henriques, E.L. Albuquerque, E.W.S. Caetano, V.N. Freire, J.A.P. da Costa, Chem. Phys. Lett. 480 (2009) 273.
[13] C.-M. Fang, R. Ahuja, Phys. Earth Planet. Interiors 157 (2006) 1.
[14] M.D. Segall, P.L.D. Lindan, M.J. Probert, C.J. Pickard, P.J. Hasnip, S.J. Clark, M.C. Payne, J. Phys. Condens. Matter 14 (2002) 2717.
[15] P. Hohenberg, W. Kohn, Phys. Rev. 136 (1964) B864.
[16] W. Kohn, L.J. Sham, Phys. Rev. 140 (1965) A1133.
[17] R.O. Jones, O. Gunnarsson, Rev. Mod. Phys. 61 (1989) 689.
[18] O.V. Gritsenko, P.R. Schipper, E.J. Baerends, J. Chem. Phys. 107 (1997) 5007.
[19] A. Dal Corso, A. Pasquarello, A. Baldereschi, R. Car, Phys. Rev. B 53 (1996) 1180.
[20] M. Fuchs, M. Bockstedte, E. Pehlke, M. Scheffler, Phys. Rev. B 57 (1998) 2134.
[21] J.P. Perdew, A. Zunger, Phys. Rev. B 23 (1981) 5048.
[22] D.M. Ceperley, B.J. Alder, Phys. Rev. Lett. 45 (1980) 566.
[23] J.P. Perdew, K. Burke, M. Ernzerhof, Phys. Rev. Lett. 77 (1996) 3865.
[24] J.P. Perdew, J.A. Chevary, S.H. Vosko, K.A. Jackson, M.R. Pederson, D.J. Singh, C. Fiolhais, Phys. Rev. B 46 (1992) 6671.
[25] D. Vanderbilt, Phys. Rev. B 41 (1990) 7892.
[26] H.J. Monkhorst, J.D. Pack, Phys. Rev. B 13 (1976) 5188.
[27] B.G. Pfrommer, M. Cote, S.G. Louie, M.L. Cohen, J. Comput. Phys. 131 (1997) 233.
[28] J.S. Lin, A. Qteish, M.C. Payne, V. Heine, Phys. Rev. B 47 (1993) 4174.
[29] S. Sasaki, T. Prewitt, R.C. Liebermann, Am. Miner. 68 (1983) 1189.
[30] R.W. Godby, M. Schlüter, L.J. Sham, Phys. Rev. B 37 (1988) 10159.
[31] J.P. Perdew, M. Levy, Phys. Rev. Lett. 51 (1983) 1884.
[32] Z.H. Levine, D.C. Allan, Phys. Rev. B 43 (1991) 4187.
[33] U. Schönberger, F. Aryasetiawan, Phys. Rev. B 52 (1995) 8788.
[34] S.Q. Wang, H.Q. Ye, J. Phys. Condens. Matter 15 (2003) L197.
[35] D.B. Migas, L. Miglio, V.L. Shaposhnikov, V.E. Borisenko, Phys. Rev. B 67 (2003) 205203.
[36] S. Lebègue, B. Arnaud, M. Alouani, Phys. Rev. B 72 (2005) 085103.
[37] D.I. Bilc, R. Orlando, R. Shaltaf, G.-M. Rignanese, J. Íñiguez, Ph. Ghosez, Phys. Rev. B 77 (2008) 165107.
[38] B. Arnaud, M. Alouani, Phys. Rev. B 63 (2001) 085208.
[39] S. Saha, T.P. Sinha, A. Mookerjee, Eur. Phys. J. B 18 (2000) 207.
[40] H.A. Kramers, Nature 117 (1926) 775.
[41] R.L. de Kronig, J. Opt. Soc. Am. 12 (1926) 547.
[42] Y. Liu, B. Lei, C. Shi, Chem. Mater. 17 (2005) 2108.
[43] J. Kuang, Y. Liu, B. Lei, C. Shi, J. Mater. Chem. 15 (2005) 4025.
[44] J. Kuang, Y. Liu, B. Lei, J. Luminescence 118 (2006) 33.